El Niño-Southern Oscillation frequency cascade
SI Appendix

Malte F. Stuecker[1,†],
Fei-Fei Jin[1],
Axel Timmermann[2]

1. Department of Atmospheric Sciences, SOEST, University of Hawai'i at Mānoa, Honolulu, HI, USA.

2. IPRC, SOEST, University of Hawai'i at Mānoa, Honolulu, HI, USA.

[†]stuecker@soest.hawaii.edu

SI Materials and Methods

Signal to noise ratio

The coefficient of determination (R^2) is calculated for each experiment between the NWP-AC(t) index and the ensemble mean $\overline{\text{NWP-AC(t)}}$ index, as an estimation of the signal to noise ratio and the maximum potential predictability of the anomalous NWP circulation (Table S5). The explained variance (R^2) by the ensemble mean is between 35% and 55%. Note that we would expect a considerable lower potential predictability in the observations, due to the broad interannual spectral peak of ENSO in reality. Additionally, our idealized sinusoidal frequency experiments have a relatively large forcing amplitude (the amplitude of the Niño 3.4 (N3.4) SSTA index, calculated as a box average of HadISST1 [2] SSTA in the area from 170°W-120°W and 5°S-5°N, is 2.46°C in the idealized experiments) and by definition no extended ENSO-neutral conditions, which we frequently find in the observations. The residuals (NWP-AC(t)$-\overline{\text{NWP-AC(t)}}$) all have white noise characteristics with no significant autocorrelation.

Reconstructions for the individual frequency experiments

The linear correlation coefficients (R) between our reconstructions and the ensemble mean indices $\overline{\text{NWP-AC(t)}}$ are displayed in Table S3. Only a very small fraction of the variance is explained by the linear ENSO term (Ψ_a). Once the quadratic C-mode interaction term and the quadratic ENSO term are added (Ψ_b), most of the variance in the signal can be explained. Adding the cubic terms (Ψ_c) further improves the correlation (as expected from the spectra (Figs. S2a,S3a,S4a)). Note that we would expect a natural increase in the explained variance by adding additional degrees of freedom for the optimization. However, the fact that we estimate very similar regression coefficients for the cubic terms independent of the ENSO forcing frequency, gives us confidence that this increase in explained variance is not artificial. Due to the frequency overlapping issue (Table S1), adding the cubic term for the 2 year period experiment actually decreases the correlation between the ensemble mean index and the optimization (Table S3).

We calculate the cross spectra (using the Welch method [3]) between the ensemble mean circulation index $\overline{\text{NWP-AC(t)}}$ and the optimized theoretical reconstructions (using all the terms in the equations above) for the 3/10 y^{-1}, 3/13 y^{-1}, and 3/16 y^{-1} frequency experiments. For the previously identified peaks (Figs. S2a,S3a,S4a), we find also a very good agreement for the estimated phase (Figs. S2b,S3b,S4b) and the magnitude squared coherence (Figs. S2c,S3c,S4c). This result is in agreement with our hypothesis that the deterministic signal in the anomalous circulation index can be attributed to the direct ENSO response, and more importantly to the different ENSO/annual cycle interaction terms. Note that we observe also peaks at $3\pm f_E$ in the $\overline{\text{NWP-AC(t)}}$ spectra (Figs. S2a,S3a,S4a), which are not included in our optimization as we only consider the quadratic and cubic interaction terms.

AGCM experiment with 1958-2013 SSTA forcing

We design an AGCM experiment that utilizes the same ENSO SSTA pattern as the idealized frequency experiments, however this time the spatio-temporal evolution is derived by multiplying the ENSO pattern with the observed 1958-2013 N3.4 SSTA index. We then integrate 20 ensemble members to estimate the atmospheric noise and separate it from the signal. In contrast to the idealized sinusoidal experiments, we expect a less strong signal as there are extended periods between 1958-2013 that are ENSO-neutral or only exhibit very weak El Niño or La Niña conditions. Additionally, we test if the JRA-55 reanalysis [1] captures the higher order combination tones as well.

To calculate the theoretical reconstruction time series, we utilize the averaged regression coefficients from the idealized experiments and use all the terms as done previously (Table S2). Using the time period from 1958 to 2013, we compare the anomalous low-level NWP-AC(t) index for the JRA-55 reanalysis [1], the ensemble mean $\overline{\text{NWP-AC(t)}}$ index from the AGCM experiment, and the reconstructed time series that includes both the ENSO and C-mode terms.

When analyzing the 1958-2013 model experiment, we find that only ∼19% of the anomalous NWP circulation variance can be explained by a deterministic signal, the rest is atmospheric noise (R^2(NWP-AC(t),$\overline{\text{NWP-AC(t)}}$) = 0.19). This can be explained by the smaller amplitude of the SSTA forcing in this experiment compared to the idealized single frequency experiments. In the observations, extended ENSO-neutral conditions persist during which the anomalous NWP circulation is only comprised of internal atmospheric variability.

Supplementary Tables

Table S 1: Rounded model experiment forcing and interaction frequencies [y^{-1}], as well as ensemble size (number of repeated cycles with same ENSO and annual cycle phase).

f_E	$2f_E$	$3f_E$	$1-f_E$	$1+f_E$	$1-2f_E$	$1+2f_E$	$2-f_E$	$2+f_E$	ensemble size
0.19 (3/16)	0.38	0.56	0.81	1.19	0.62	1.38	1.81	2.19	20
0.23 (3/13)	0.46	0.69	0.77	1.23	0.54	1.46	1.77	2.23	20
0.25 (1/4)	0.50	0.75	0.75	1.25	0.50	1.50	1.75	2.25	30
0.30 (3/10)	0.60	0.90	0.70	1.30	0.40	1.60	1.70	2.30	20
0.33 (1/3)	0.67	1.00	0.67	1.33	0.33	1.67	1.67	2.33	30
0.40 (2/5)	0.80	1.20	0.60	1.40	0.20	1.80	1.60	2.40	20
0.43 (3/7)	0.86	1.29	0.57	1.57	0.14	1.86	1.57	2.43	10
0.50 (1/2)	1.00	1.50	0.50	1.50	0.00	2.00	1.50	2.50	30

Table S 2: Estimated optimization coefficients for the individual experiments and the mean of the coefficients for the experiment with non-overlapping response frequencies. The units for the amplitude coefficients α are either $[10^6 \mathrm{m}^2\mathrm{s}^{-1}{}^\circ\mathrm{C}^{-1}]$ or $[10^6 \mathrm{m}^2\mathrm{s}^{-1}{}^\circ\mathrm{C}^{-2}]$, while the units for the phase coefficients ϕ are [mo].

Exp. freq. f_E [y^{-1}]	α_{10}	α_{20}	α_{11}	ϕ_1	α_{21}	ϕ_2	α_{12}
0.19 (3/16)	-0.13	-0.12	0.54	2.83	0.13	4.22	0.24
0.23 (3/13)	-0.08	-0.12	0.54	2.90	0.14	4.38	0.30
0.25 (1/4)	-0.09	-0.12	0.50	2.80	0.17	3.88	0.21
0.30 (3/10)	-0.08	-0.11	0.52	2.77	0.14	4.45	0.27
0.33 (1/3)	-0.09	-0.04	0.45	3.22	0.10	4.70	0.08
0.40 (2/5)	-0.10	-0.10	0.50	2.73	0.10	4.47	0.22
0.43 (3/7)	-0.08	-0.12	0.45	2.80	0.14	4.66	0.16
0.50 (1/2)	0.40	0.00	0.34	3.35	0.00	5.42	0.30
mean (non-overlap)	-0.09	-0.11	0.51	2.81	0.13	4.44	0.24

Table S 3: Linear correlation coefficients (R) between the ensemble mean $\overline{\text{NWP-AC(t)}}$ indices and the time series reconstructions (Ψ) using the averaged coefficients. Ψ_a includes only the linear ENSO term. Ψ_b includes the linear ENSO term and the quadratic interaction and non-interaction terms. Ψ_c includes all the aforementioned terms plus the cubic interaction terms.

Exp. freq. f_E [y^{-1}]	R(index,Ψ_a)	R(index,Ψ_b)	R(index,Ψ_c)
0.19 (3/16)	0.27	0.89	0.93
0.23 (3/13)	0.28	0.85	0.91
0.25 (1/4)	0.21	0.88	0.93
0.30 (3/10)	0.25	0.87	0.92
0.33 (1/3)	0.22	0.92	0.93
0.40 (2/5)	0.31	0.89	0.92
0.43 (3/7)	0.30	0.87	0.91
0.50 (1/2)	0.11	0.85	0.84

Table S 4: Comparison between the amplitude coefficients $\alpha_{n(k-n)}$ estimated from the idealized frequency experiments and the multiple linear regression approach for the low-pass filtered JRA-55 NWP-AC(t) index. The phases for the annual cycle and semi-annual cycle are fixed to the previously estimated values.

$\alpha_{n(k-n)}$	term	mean (non-overlapping Exp.)	JRA-55 regression estimates
α_{10} $[10^6 \mathrm{m^2 s^{-1} {}^\circ C^{-1}}]$	E	-0.09	-0.07
α_{20} $[10^6 \mathrm{m^2 s^{-1} {}^\circ C^{-2}}]$	E^2	-0.11	0.19
α_{11} $[10^6 \mathrm{m^2 s^{-1} {}^\circ C^{-1}}]$	E x A	0.53	0.82
α_{21} $[10^6 \mathrm{m^2 s^{-1} {}^\circ C^{-2}}]$	E^2 x A	0.13	-0.01
α_{12} $[10^6 \mathrm{m^2 s^{-1} {}^\circ C^{-1}}]$	E x SA	0.24	0.26

Table S 5: The deterministic signal of the anomalous NWP-AC circulation defined as $R^2(\text{NWP-AC(t)}, \overline{\text{NWP-AC(t)}})$.

Experiment frequency f_E $[\mathrm{y^{-1}}]$	$R^2(\text{NWP-AC(t)}, \overline{\text{NWP-AC(t)}})$
0.19 (3/16)	0.51
0.23 (3/13)	0.53
0.25 (1/4)	0.45
0.30 (3/10)	0.51
0.33 (1/3)	0.42
0.40 (2/5)	0.50
0.43 (3/7)	0.55
0.50 (1/2)	0.35

Supplementary Figures

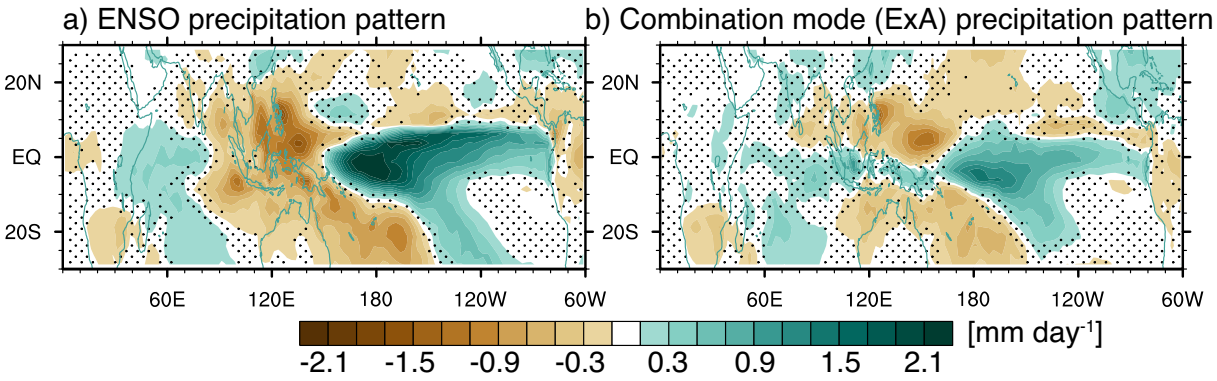

Fig. S 1: Schematic for the ENSO (E) and combination mode (ExA) anomalous precipitation pattern. **(a)** Regression coefficient of the normalized N3.4 index and the anomalous GPCP V2.2 [4] precipitation for the period 1979-2013 (ENSO pattern). **(b)** Regression coefficient of the normalized combination mode (ExA) index and the anomalous GPCP V2.2 [4] precipitation for the same period (combination mode pattern). Areas where the anomalous precipitation regression coefficient is significant above the 95% confidence level are non-stippled.

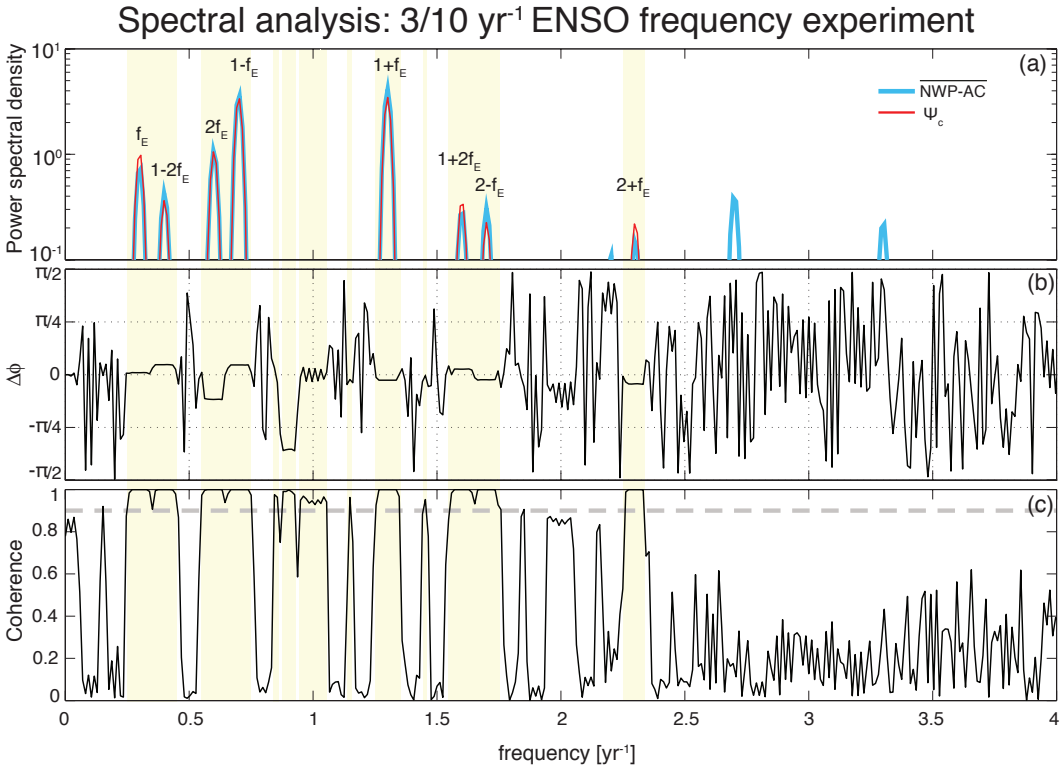

Fig. S 2: Spectral analysis for the 3/10 y^{-1} ENSO frequency experiment. The forcing frequency (f_E), the first overtone ($2f_E$), quadratic ($1 - f_E$, $1 + f_E$), and cubic combination tones ($1 - 2f_E$, $1 + 2f_E$, $2 - f_E$, $2 + f_E$) are labeled. **a)** Power spectral density for the $\overline{\text{NWP-AC(t)}}$ index (blue) and the reconstruction (red) using the Welch method. **b)** Phase difference between the two time series. **c)** Magnitude squared coherence between the two time series. The frequency bands with a coherence above 0.9 (dashed gray line) are indicated by yellow shading.

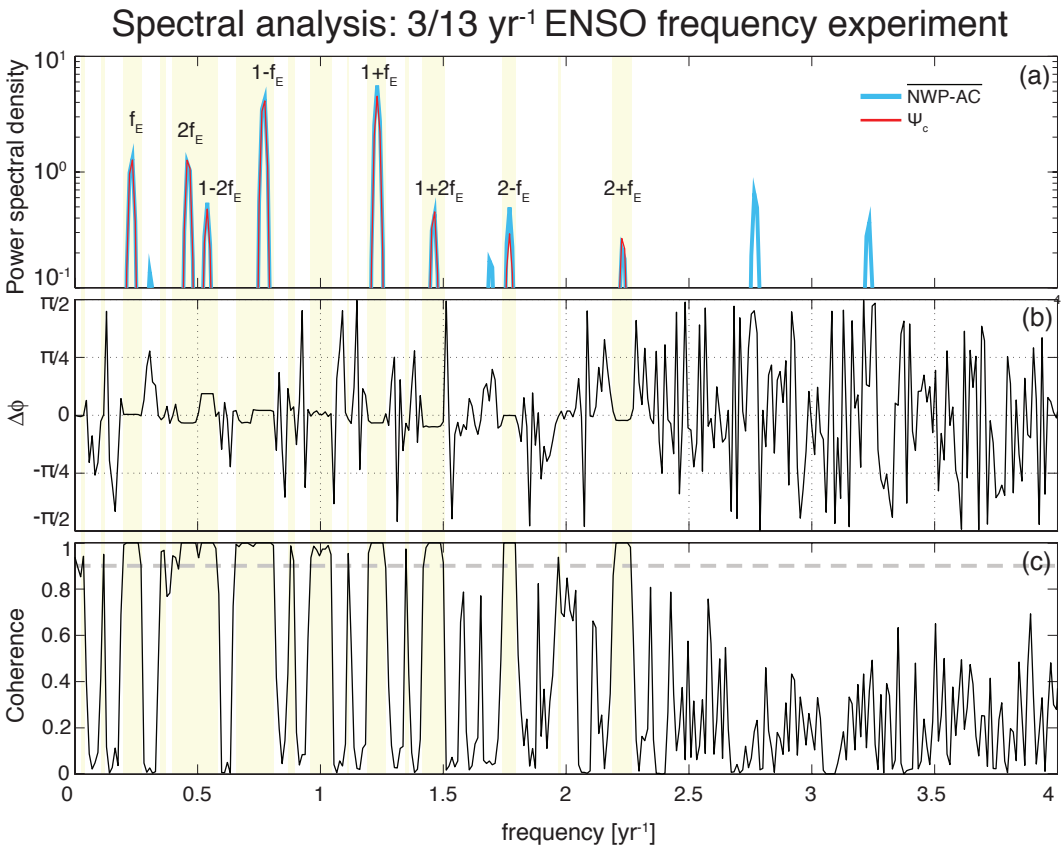

Fig. S 3: Spectral analysis for the 3/13 y^{-1} ENSO frequency experiment. The forcing frequency (f_E), the first overtone ($2f_E$), quadratic ($1 - f_E$, $1 + f_E$), and cubic combination tones ($1 - 2f_E$, $1 + 2f_E$, $2 - f_E$, $2 + f_E$) are labeled. **a)** Power spectral density for the $\overline{\text{NWP-AC(t)}}$ index (blue) and the reconstruction (red) using the Welch method. **b)** Phase difference between the two time series. **c)** Magnitude squared coherence between the two time series. The frequency bands with a coherence above 0.9 (dashed gray line) are indicated by yellow shading.

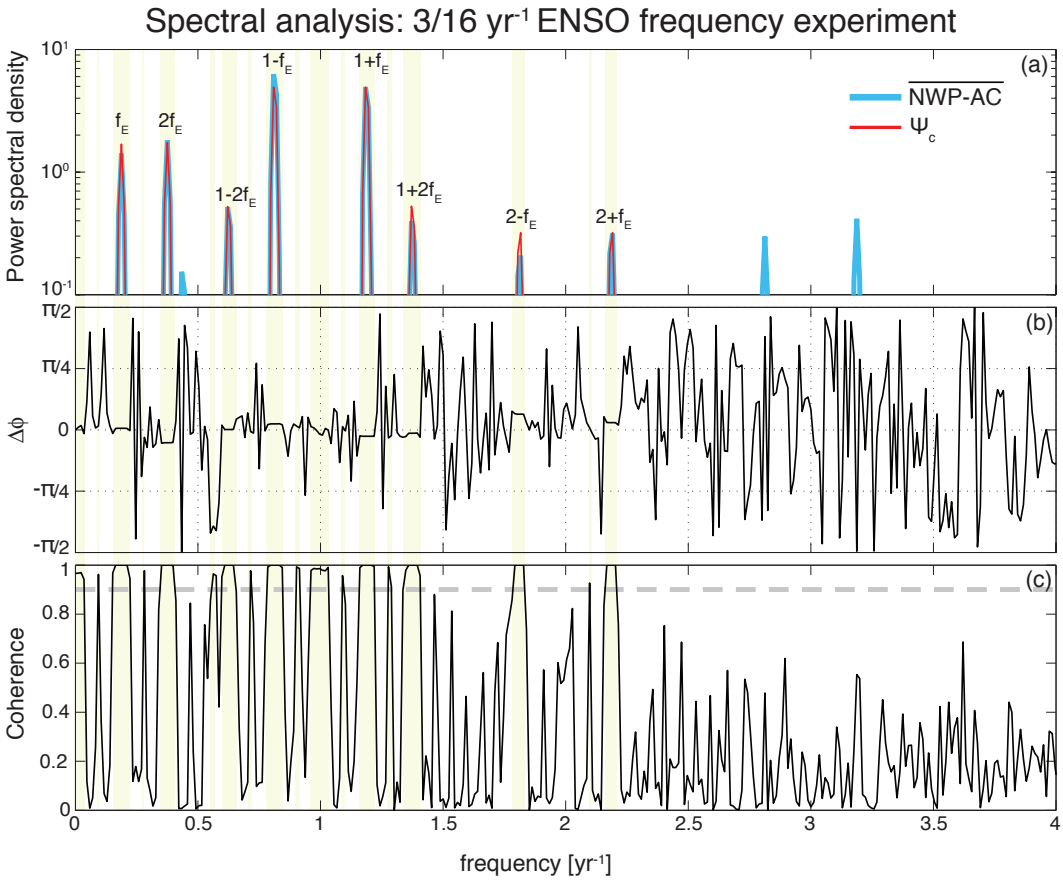

Fig. S 4: Spectral analysis for the 3/16 y^{-1} ENSO frequency experiment. The forcing frequency (f_E), the first overtone ($2f_E$), quadratic ($1 - f_E$, $1 + f_E$), and cubic combination tones ($1 - 2f_E$, $1 + 2f_E$, $2 - f_E$, $2 + f_E$) are labeled. **a)** Power spectral density for the $\overline{\text{NWP-AC(t)}}$ index (blue) and the reconstruction (red) using the Welch method. **b)** Phase difference between the two time series. **c)** Magnitude squared coherence between the two time series. The frequency bands with a coherence above 0.9 (dashed gray line) are indicated by yellow shading.

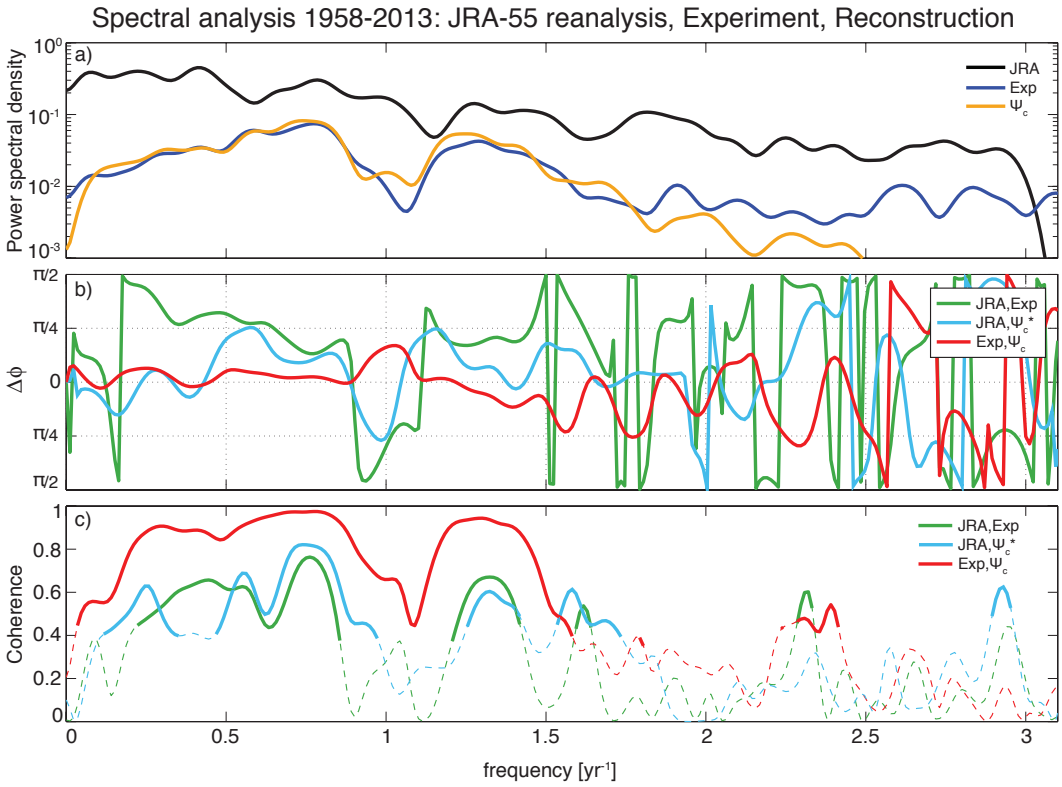

Fig. S 5: Spectral analysis for the 1958-2013 time period using the anomalous NWP-AC circulation indices for the JRA-55 reanalysis (black), the 20 member ensemble mean AGCM experiment (dark blue), and the theoretical reconstruction including both the ENSO and C-mode terms (orange). The model is compared to the reconstruction using the averaged estimated coefficients (Ψ_c), while the JRA-55 index is compared with the reconstruction using the regressed coefficients (Ψ_c*). **a)** Power spectral density for the NWP-AC(t) indices using the Welch method. **b)** Phase difference between the respective time series: reanalysis and experiment (green), reanalysis and reconstruction (light blue), reconstruction and experiment (red). **c)** Magnitude squared coherence for the above time series pairs. Statistical significance is inferred using bootstrapping (n=1000) and the coherence above (below) the 95% confidence level is indicated by solid (dashed) lines.

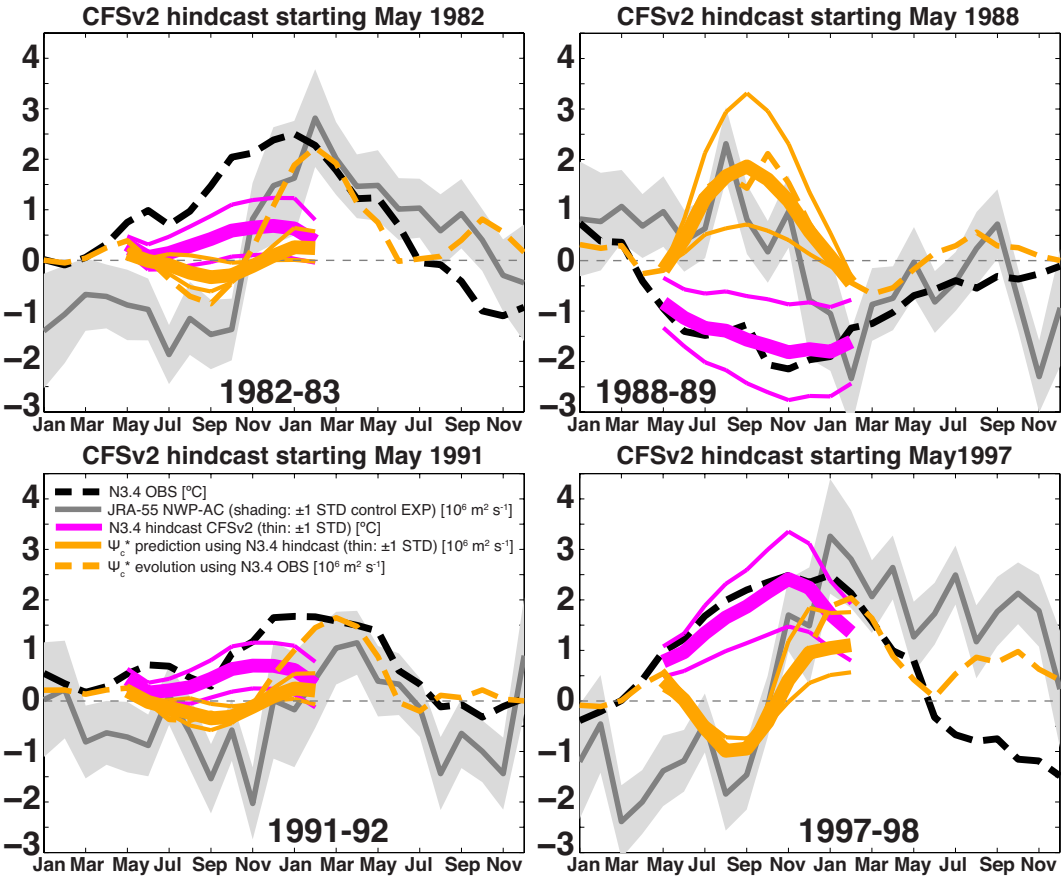

Fig. S 6: Predictability of the observed NWP-AC circulation during major El Niño and La Niña events. Shown are the observed N3.4 index (dashed black line), the JRA-55 NWP-AC index (solid gray line), and the CFSv2 hindcast for the N3.4 index beginning in May (onset phase) of each event (thick magenta line). The error estimate for the NWP-AC index is one standard deviation (SD) of the NWP-AC circulation in a 50 year integration of CESM CAM4 with only the annual cycle as forcing (gray shading). The error for the N3.4 hindcast is one SD in the ensemble spread (thin magenta lines). The reconstruction Ψ_c* is used for predicting the circulation (solid orange line for the prediction and thin orange lines for the one SD error) and on the observations (dashed orange line). A small offset between observations and the CFSv2 initialization is explained by both the CFSv2 climatology (1999-2010) and the observational uncertainty of the CFSv2 analysis (the standard deviation of the initial conditions is shown by the range of the thin magenta lines during the first month).

SI References

1. Kobayashi S, et al. (2015) The JRA-55 Reanalysis: General Specifications and Basic Characteristics. *Journal of the Meteorological Society of Japan* doi: 10.2151/jmsj.2015-001.

2. Rayner NA, et al. (2003) Global analyses of sea surface temperature, sea ice, and night marine air temperature since the late nineteenth century. *J. Geophys. Res.* 108(D14) doi:10.1029/2002JD002670.

3. Welch PD (1967) The Use of Fast Fourier Transform for the Estimation of Power Spectra: A Method Based on Time Averaging Over Short, Modified Periodograms. *IEE Trans. Audio and Electroacoust.* AU-15:70–73.

4. Adler RF, et al. (2003) The Version-2 Global Precipitation Climatology Project (GPCP) monthly precipitation analysis (1979-present). *J. Hydrometeor.* 4:1147-1167.